Theoretical Study on Hydrozirconation

Jun Endo,[1] Nobuaki Koga,[2a] and Keiji Morokuma*,[2b]

Institute for Molecular Science, Myodaiji, Okazaki 444, Japan, and Yokkaichi Research Center, Mitsubishi Petrochemical Company Ltd., Toho-cho, Yokkaichi 510, Japan

Received October 16, 1992

An ab initio MO study has been carried out for hydrozirconation of ethylene and acetylene by $Cp_2Zr(H)Cl$. Of the two possible reaction paths, attack of ethylene and acetylene at Zr between the Cl and H ligands (path 1) and that from the opposite side of the Cl ligand (path 2), the former is found to be more favorable, with a very low activation energy. With an energy decomposition analysis, this difference has been attributed to the smaller distortion of the Zr complex required to reach the transition state for path 1. Hydrozirconation of acetylene is intrinsically more difficult than that of ethylene. The olefin insertion at $Cp_2Zr(R)Cl$, R = alkyl, i.e. the second insertion of olefin, is substantially more difficult than hydrozirconation (R = H) the first insertion. Its origin is also discussed. For comparison, the results of hydrozirconation by Cl_3ZrH have been presented, to clarify the size effect of Cp ligand.

1. Introduction

Hydrozirconation is an olefin insertion reaction at a Zr–H bond, first discovered in 1974 for $Cp_2Zr(H)Cl$.[3] Since then, zirconocene catalysts have been frequently applied in organic synthesis.[4] Hydrozirconation follows the anti-Markovnikov and the cis addition rule and allows introduction of various substituents at the olefin, just like hydroboration. For example, treatment of the hydrozirconation product with acid and bromine gives the corresponding hydrocarbon and alkyl bromide, respectively. Carbon monoxide inserts into the Zr–C bond of the product, to give an aldehyde and a carboxylic acid as a result of reaction with acid and water, respectively. One interesting aspect is that a four-centered, concerted transition state is symmetry-allowed in hydrozirconation, in which the Zr atom has formally-vacant d orbitals available,[5] whereas that for a reaction without a d orbital, such as hydroboration, is formally symmetry-forbidden, though the calculated barrier for the latter is actually very low.[6]

Hydrozirconation, a relatively simple reaction, can also serve as a model reaction for olefin polymerization catalyzed by the homogeneous catalyst first reported by Kaminsky et al.[7] This catalyst consists of Cp_2ZrCl_2 and methylaluminoxane in general and gives syndiotactic, as well as isotactic, polymers using suitable ligands,[8] a feature not found in Ziegler–Natta catalysts. Neither the active species nor the reaction mechanism of the Kaminsky type polymerization is fully established. A popular current thought is that the active species in the polymerization is a cationic complex such as $Cp_2Zr^{IV}R^{+9}$ and that the reaction proceeds through a four-centered transition state as in the Cossee mechanism[10] for the Ziegler–Natta catalysis. Some theoretical studies have been reported on this cationic complex.[11,12] Christ et al. have shown, however, that Cp_2ZrR^+ does not cause polymerization in the gas phase and offered a model of the active species, Cp_2ZrR^+, coordinated at Zr by several solvent molecules.[13]

As far as the authors are aware, there is no theoretical investigation for hydrozirconation. In the present paper we report the results of an ab initio MO study of hydrozirconation of ethylene (reaction 1) and acetylene

$$Cp_2Zr(H)Cl + C_2H_4 \rightarrow Cp_2Zr(C_2H_5)Cl \quad (1)$$

$$Cp_2Zr(H)Cl + C_2H_2 \rightarrow Cp_2Zr(C_2H_3)Cl \quad (2)$$

$$Cp_2Zr(CH_3)Cl + C_2H_4 \rightarrow Cp_2Zr(C_3H_7)Cl \quad (3)$$

(reaction 2) by $Cp_2Zr(H)Cl$ and, for comparison, the insertion reaction of ethylene into the Zr–C bond of $Cp_2Zr(CH_3)Cl$ (reaction 3). Experimentally, it is well-known that the second olefin does not insert into the Zr–C bond formed in hydrozirconation (reaction 1).[3] Reaction 3 corresponds to this insertion. For these reactions, we have determined the equilibrium and transition state geometries and energies for possible reaction paths and elucidated detailed mechanisms of reaction. In addition, we have carried out the calculations for the reaction of the

(1) Visiting Research Fellow of the Institute for Molecular Science from Mitsubishi Petrochemical Co. Ltd.

(2) Institute for Molecular Science. Present address: (a) Department of Chemistry, College of General Education, Nagoya University, Nagoya 464-01, Japan. (b) Cherry L. Emerson Center for Scientific Computation and Department of Chemistry, Emory University, Atlanta, GA 30322.

(3) (a) Hart, D. W.; Schwartz, J. *J. Am. Chem. Soc.* **1974**, *96*, 8115. (b) Labinger, J. A.; Hart, D. W.; Seibert, W. E., III; Schwartz, J. *J. Am. Chem. Soc.* **1975**, *97*, 3851. (c) Schwartz, J.; Labinger, J. A. *Angew. Chem., Int. Ed. Engl.* **1976**, *15*, 333. (d) Hart, D. W.; Blackburn, T. F.; Schwartz, J. *J. Am. Chem. Soc.* **1975**, *97*, 679.

(4) *Comprehensive Organometallic Chemistry*; Wilkinson, G., Stone, G. A., Abel, E. W., Ed.; Pergamon Press: New York, 1982; Vol. 3, Chapter 23.

(5) Koga, N.; Morokuma, K. *Chem. Rev.* **1991**, *91*, 823.

(6) Nagase, S.; Ray, N. K.; Morokuma, K. *J. Am. Chem. Soc.* **1980**, *102*, 4536.

(7) Sinn, H.; Kaminsky, W.; Vollmer, H.-J.; Woldt, R. *Angew. Chem., Int. Ed. Engl.* **1980**, *19*, 390.

(8) Ewen, J. A.; Jones, R. L.; Razavi, A.; Ferrara, J. D. *J. Am. Chem. Soc.* **1988**, *110*, 6255.

(9) (a) Gassman, P. G.; Callstrom, M. R. *J. Am. Chem. Soc.* **1987**, *109*, 7875. (b) Jordan, R. F.; Bajgur, C. S.; Willett, R.; Scott, B. *J. Am. Chem. Soc.* **1986**, *108*, 7410. (c) Bochmann, M.; Jaggar, A. J.; Nicholls, J. C. *Angew. Chem., Int. Ed. Engl.* **1990**, *29*, 780.

(10) Cossee, P. *J. Catal.* **1964**, *3*, 80.

(11) (a) Fujimoto, H.; Yamasaki, T.; Mizutani, H.; Koga, N. *J. Am. Chem. Soc.* **1985**, *107*, 6157. (b) Jolly, C. A.; Marynick, D. S. *J. Am. Chem. Soc.* **1989**, *111*, 7968. (c) Castonguay, L. A.; Rappé, A. K. *J. Am. Chem. Soc.* **1992**, *114*, 5832.

(12) (a) Kawamura-Kuribayashi, H.; Koga, N.; Morokuma, K. *J. Am. Chem. Soc.* **1992**, *114*, 2359. (b) Kawamura-Kuribayashi, H.; Koga, N.; Morokuma, K. *J. Am. Chem. Soc.* **1992**, *114*, 8687.

(13) Christ, C. S.; Jr.; Eyler, J. R.; Richardson, D. E. *J. Am. Chem. Soc.* **1990**, *112*, 596.

0276-7333/93/2312-2777$04.00/0

chloride analogue, $Cl_2Zr(H)Cl$, with C_2H_4 (reaction 4), in order to compare electronic as well as steric effects between Cp and Cl. In many previous theoretical studies the Cp ligands were replaced by Cl.[14]

$$Cl_2Zr(H)Cl + C_2H_4 \rightarrow Cl_2Zr(C_2H_5)Cl \qquad (4)$$

2. Computational Details

In optimizing the equilibrium and the transition state structures we used the restricted Hartree–Fock (RHF) energy gradient technique, with the GAUSSIAN82 program,[15] implemented with the effective core potential (ECP)[16] and the Obara integral code.[17] For the group IV transition metal d^0 complexes, the RHF wavefunction is considered to be acceptable as the reference wavefunction.[18] For better energetics, energies at the RHF optimized geometries were also calculated with the frozen-core second order Møller–Plesset perturbation method (MP2). For reaction 4, the geometry determinations at the MP2 level were also carried out by using the GAUSSIAN92 program.[19]

All the geometry optimizations were carried out under the C_s symmetry constraint. Furthermore, the Cp rings were assumed to maintain a local C_{5v} symmetry and to be perpendicular to the Zr–X axis, where X is the center of the Cp ring. The geometrical parameters of the Cp ring, the C–C and C–H distances and the X–C–H out-of-plane angle, were frozen to those optimized for our reference compound Cp_2ZrCl_2 under the C_{2v} constraint.

For the zirconium atom, the 4s to 5p valence basis functions with the ECP, determined by Hay and Wadt, were adopted[20] and contracted to (311/311/31). The 3-21G[21] basis set was used for the ethylene, acetylene, chloride, and hydride ligands, whereas the minimal STO-3G[22] basis set was used for the spectator Cp ligands. Use of a small basis set for ligands not directly involved in the relevant reaction has previously been justified.[23] This basis set is denoted by I. For reaction 4, we also used better basis sets, in order to investigate the effect of the basis functions, because the basis set I is rather small. In the second basis set (basis set II), we used the split-valence

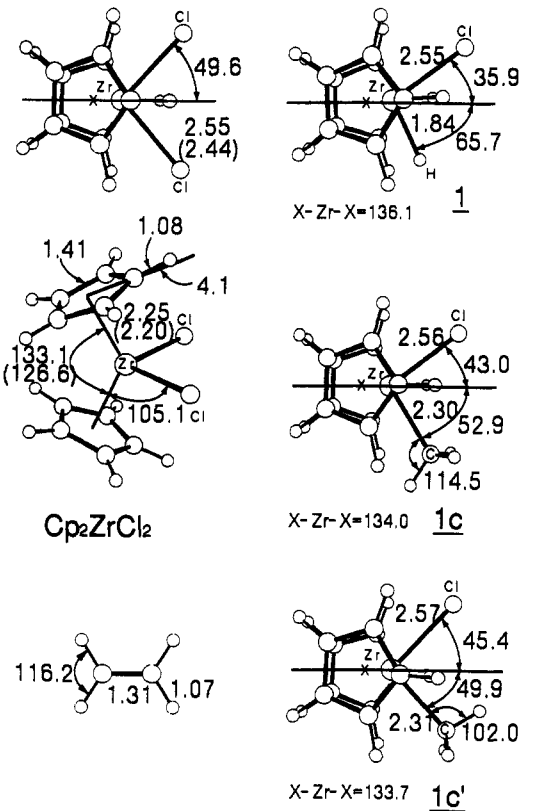

Figure 1. RHF/I optimized geometries of Cp_2ZrCl_2, $Cp_2Zr(H)Cl$ (1), and $Cp_2Zr(CH_3)Cl$ (1c and 1c′) as well as that of C_2H_4. Distances and angles are in Å and deg, respectively. Numbers in parentheses are the experimental values.[21]

(8s5p)/[3s2p], (4s)/[2s], and (11s8p)/[4s3p] basis functions for C, H, and Cl, respectively.[24] In the third basis set (III), the d polarization functions on C and Cl and the p polarization function on H[24] were added furthermore to the basis set II. For clarity, we used the standard notation to specify the level of calculation and the structure used. For instance, MP2/III//RHF/I designates an MP2 energy calculation with the basis set III using the structure determined at the RHF level with the basis set I.

3. Optimized Geometries of Cp_2ZrCl_2, $Cp_2Zr(H)Cl$, and $Cp_2Zr(CH_3)Cl$

The RHF/I optimized structure of our reference compound Cp_2ZrCl_2 is shown in Figure 1. Rigid rotation of one and both Cp ligands by 180° around the Zr–X axis at the above optimized geometry gives the staggered form and the other eclipsed form, which are more stable by 0.3 kcal/mol and less stable by 1.3 kcal/mol, respectively. This suggests that the staggered form is the most stable but both Cp ligands can rotate almost freely. X-ray diffraction has shown that Cp_2ZrCl_2 has a staggered form.[25] It is interesting to note here that such a free rotation would allow the Cp rings to rotate to reduce the steric repulsion during the reaction, as will be found later. If the Cp rings are connected by a bridge such as SiR_2, such a rotation would be prohibited which may affect some aspects of the chemistry.[12b] The theoretical value of the X–Zr–X angle is larger by 4.8–7.1° than the experimental value of 126.0–128.3°, probably partly because it is calculated for a less

(14) (a) Steigerwald, M. L.; Goddard, W. A. *J. Am. Chem. Soc.* **1985**, *107*, 5027. (b) Upton, T. H.; Rappé, A. K. *J. Am. Chem. Soc.* **1985**, *107*, 1206. (c) Koga, N.; Morokuma, K. *J. Am. Chem. Soc.* **1988**, *110*, 108. (d) Kawamura-Kuribayashi, H.; Koga, N.; Morokuma, K. *J. Am. Chem. Soc.* **1992**, *114*, 2359. (e) Castonguay, L. A.; Rappé, A. K. *J. Am. Chem. Soc.* **1992**, *114*, 5832.

(15) Binkley, J. S.; Frisch, M. J.; Defrees, D. J.; Raghavachari, K.; Whiteside, R. A.; Schlegel, H. B.; Pople, J. A. *GAUSSIAN82*; Carnegie-Mellon Chemistry Publishing Unit: Pittsburg, PA, 1984.

(16) (a) McMurchie, L. E.; Davidson, E. R. *J. Comput. Phys.* **1981**, *44*, 289. (b) Martin, R. L. Unpublished results.

(17) (a) Obara, S.; Saika, A. *J. Chem. Phys.* **1986**, *84*, 3963. (b) *Ibid.* **1988**, *89*, 1540.

(18) Cundari, T. R. *J. Am. Chem. Soc.* **1992**, *114*, 10557.

(19) Frisch, M. J.; Head-Gordon, M.; Trucks, G. W.; Foresman, J. B.; Schlegel, H. B.; Raghavachari, K.; Robb, M.; Binkley, J. S.; Gonzalez, C.; Defrees, D. J.; Fox, D. J.; Whiteside, R. A.; Seeger, R.; Melius, C. F.; Baker, J.; Martin, R. L.; Kahn, L. R.; Stewart, J. J. P.; Topiol, S.; Pople, J. A. *GAUSSIAN92*; Gaussian, Inc., Pittsburgh PA, 1992.

(20) Hay, P. J.; Wadt, W. R. *J. Chem. Phys.* **1985**, *82*, 299.

(21) Binkley, J. S.; Pople, J. A.; Hehre, W. J. *J. Am. Chem. Soc.* **1980**, 102, 939.

(22) Hehre, W. J.; Stewart, R. F.; Pople, J. A. *J. Chem. Phys.* **1969**, *51*, 2657.

(23) (a) Obara, S.; Kitaura, K.; Morokuma, K. *J. Am. Chem. Soc.* **1984**, *106*, 7482. (b) Koga, N.; Obara, S.; Kitaura, K.; Morokuma, K. *J. Am. Chem. Soc.* **1985**, *107*, 7109. (c) Koga, N.; Morokuma, K. *J. Am. Chem. Soc.* **1985**, *107*, 7230. (d) Koga, N.; Morokuma, K. *J. Am. Chem. Soc.* **1986**, *108*, 6136. (e) Koga, N.; Jin, S.-Q.; Morokuma, K. *J. Am. Chem. Soc.* **1988**, *110*, 3417. (f) Daniel, C.; Koga, N.; Han, J.; Fu, X. Y.; Morokuma, K. *J. Am. Chem. Soc.* **1988**, *110*, 3773. (g) Koga, N.; Morokuma, K. *Organometallics* **1991**, *10*, 946. (h) Koga, N.; Morokuma, K. *New J. Chem.* **1991**, *15*, 749.

(24) Huzinaga, S.; Andzelm, J.; Klbukowski, M.; Radzio-Andzelm, E.; Sakai, Y.; Tatewaki, H. *Gaussian Basis Sets for Molecular Calculations*; Elsevier: Amsterdam, 1984.

(25) Prout, K.; Cameron, T. S.; Forder, R. A.; Critchlay, S. R.; Denton, B.; Rees, G. V. *Acta Crystallogr.* **1974**, *B30*, 2290.

Scheme I

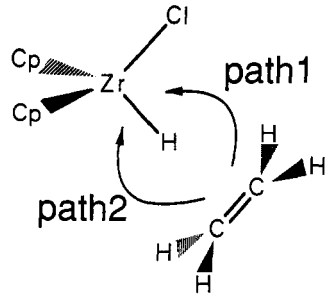

stable eclipsed form and partly because we used the poor basis functions for the Cp ligands. While the calculated Zr–X distances of 2.25 Å are very close to the experimental mean value of 2.19–2.21 Å,[25] the Zr–Cl distances were calculated to be 0.1 Å longer than the experimental value of 2.44–2.45 Å. Such long bond distances involving Cl have been obtained at the RHF level with the 3-21G basis set; for instance, the C–Cl bond distance of 1.892 Å in CH_3Cl at the RHF/3-21G level is compared with the experimental bond length of 1.781 Å.[26] This artificially long Zr–Cl bond is common in all the complexes calculated in the present paper and its effects on comparison among different substrates is expected to be negligible. Actually, it will be shown later that it is true for reaction 4.

The optimized geometries of the reactants of the present reactions, $Cp_2Zr(H)Cl$ (1) and $Cp_2Zr(CH_3)Cl$, are shown also in Figure 1. No experimental geometries are available for them. However, the calculated Zr–CH_3 distance is very close to the experimental Zr–C distance, for instance, in $(\eta^5\text{-}C_9H_7)_2Zr(CH_3)_2$ (2.251 Å) and in $Cp_2Zr(CH_2CMe_3)_2$ (2.288 Å).[27] Of two CH_3 conformations of $Cp_2Zr(CH_3)Cl$, the trans form (**1c**) is more stable than the cis form (**1c'**) by 2.4 kcal/mol, presumably because in **1c** the Zr–Cl bond is staggered to the C–H bonds of CH_3.

4. Hydrozirconation of Ethylene

For reaction 1, one can consider two paths of olefin approach depicted in Scheme I. In path 1, ethylene attacks between the hydride and the chloride ligand, whereas in path 2, it attacks from the opposite side of chloride. In both paths, the ethylene C=C bond is assumed to be coplanar with the HZrCl plane; any structure with the C=C bond perpendicular to the HZrCl plane is unstable due to a large steric repulsion between the C—H bonds of Cp and those of ethylene. The third path with the ethylene attack from the opposite side of hydride is not considered, since it does not lead to the interaction of olefin with hydride required for hydrozirconation. An extensive search for a π complex for path 1 failed, and one has to conclude that such a complex does not exist, except for a possible very weak van der Waals complex which the RHF geometry optimization may be unable to find. Olefin coordination is usually explained in terms of donation and back-donation. In an early transition metal complex, especially a neutral complex, because of a small electronegativity of the central metal, donation is difficult to take place and back-donation is expected to be responsible for olefin coordination. For instance, in ethylene coordination to d^2 Cp_2Zr^{II}, large back-donation takes place to break the CC π bond. Our calculation of $Cp_2Zr(C_2H_4)$ gave the CC bond length of 1.501 Å at the RHF/I level, which is close to the CC distance in cyclopropane (1.513 Å at the RHF/3-21G level). The Zr–C bond distances in $Cp_2Zr(C_2H_4)$ (2.27 Å) are similar to the Zr–CH_3 bond distances in **1c** and **1c'** and are much shorter than the Zr–C distances (2.9 Å) in a cationic π complex, $(H_2Si\text{-}Cp_2)Zr^{IV}(C_2H_4)(CH_3)^+$,[12b] in which donation to the electron deficient transition metal is responsible for ethylene coordination. These computational results suggest that $Cp_2Zr(C_2H_4)$ can be considered to be zirconacyclopropane, as shown.

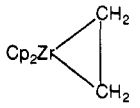

Therefore, ethylene coordination to d^2 Cp_2Zr should be regarded as an oxidative addition resulting in d^0 $Cp_2\overline{Zr\text{-}CH_2CH_2}$. A similar conclusion has been obtained in the theoretical analysis of the interaction between Cl_2Ti and C_2H_4 by Steigerwald and Goddard.[28] On the other hand, our reactant is 1 with d^0 Zr^{IV} and thus oxidatively additive ethylene coordination to 1 is not feasible.

The RHF/I optimized structures of the transition states (**21a** and **22a**), direct products (**31a** and **32a**), and final product (**41a** and **42a**) are shown in Figure 2.[29] The direct products are the products of reaction throughout which C_s symmetry is maintained, and the final products are those in which the product methyl group is allowed to rotate to the most stable conformation. For olefin insertion at a d^0 titanium complex $CH_3TiCl_2^+$, a twisted transition state with a C_1 symmetry has been found.[12a] To investigate this possibility, we also optimized the geometry of **21a** starting from an initial guess of C_1 symmetry, to obtain the same C_s transition state shown in Figure 2. We note here that the transition state for olefin insertion to d^0 $(H_2SiCp_2)ZrCH_3^+$ has been calculated to be nearly C_s-symmetric.[12b]

In both transition states **21a** and **22a** the Zr—H and the C=C distances are only 2% and 4–5%, respectively, longer than those in the reactants. On the other hand, the newly forming Zr—C and C—H bonds are still 10–16% and 57–70%, respectively, longer than those in the products. Thus the transition states are in a very early stage of reaction. The new bond formation at the transition states is asynchronous in the aspect that the Zr—C bond formation is more advanced than formation of the C—H bond which is still very long. Comparing the transition state **21a** for path 1 with that **22a** for path 2, one finds that **21a** for path 1 is located later on the reaction coordinate than **22a**. The Cp ligands in **22a** have rotated from the structure of 1 by about 36° around the Zr—X axis, presumably to minimize the repulsion between the hydrogen atoms of Cp and those of ethylene. The facile rotation of the Cp ligands in 1, noted in section 3, is in operation here.

In Figure 3 are shown the potential energy profiles at both the RHF/I//RHF/I and MP2/I//RHF/I levels. The electron correlation effect lowers the activation energy by about 15 kcal/mol and increases the exothermicity by about

(26) Gordon, M. S.; Binkley, J. S.; Pople, J. A.; Pietro, W. J.; Hehre, W. J. *J. Am. Chem. Soc.* **1982**, *104*, 2797.

(27) (a) Atwood, J. L.; Hunter, W. E.; Hrncir, D. C.; Samuel, E.; Alt, H.; Rausch, M. D. *Inorg. Chem.* **1975**, *14*, 1757. (b) Jeffery, J.; Lappert, M. F.; Luong-Thi, N. T.; Atwood, J. L.; Hunter, W. E. *J. Chem. Soc., Chem. Commun.* **1978**, 1081.

(28) Steigerwald, M. L.; Goddard, W. A., III. *J. Am. Chem. Soc.* **1985**, *107*, 5027.

(29) Our numbering system is as follows. For the first character, 1–4 designate a reactant, a transition state, a direct product, and a final product, respectively. The second character specifies the path. The third character designates a reaction: a–d for reactions 1–4, respectively.

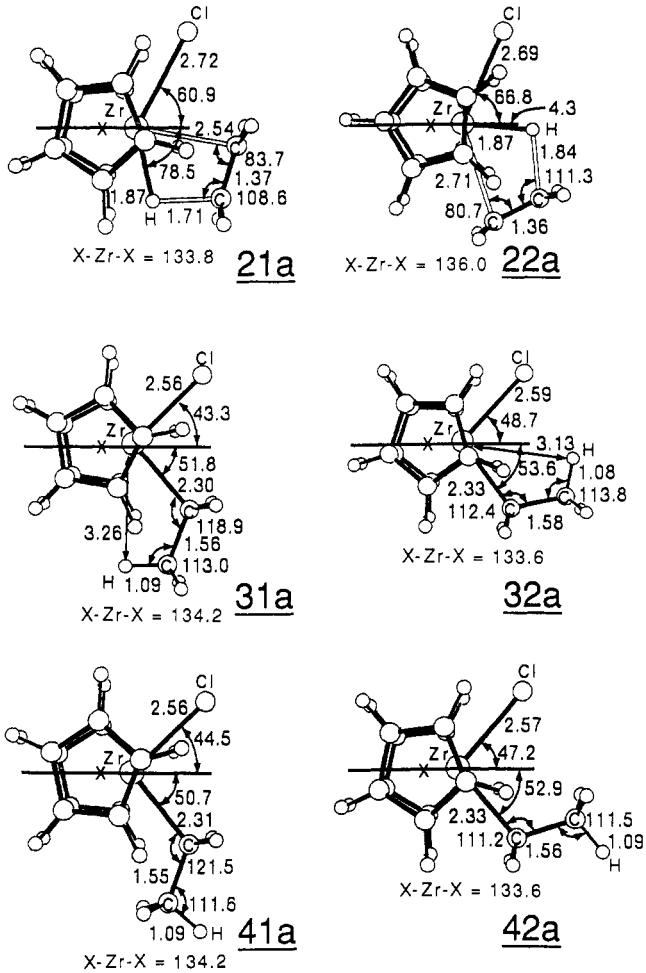

Figure 2. RHF/I optimized geometries of transition states (**21a** and **22a**), direct products (**31a** and **32a**), and final products (**41a** and **42a**) for paths 1 and 2, respectively, of the hydrozirconation of ethylene. Distances and angles are in Å and deg, respectively.

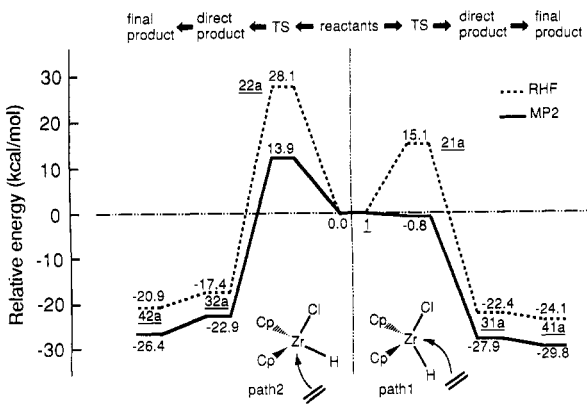

Figure 3. Relative energies of the transition states and direct and final products for the hydrozirconation of ethylene. The RHF/I//RHF/I (MP2/I//RHF/I) energies in hartrees for 1 and ethylene are −884.01729 (−884.76830) and −77.60099 (−77.78013), respectively.

5 kcal/mol for both paths. Of the two paths, the more favorable is path 1 at both levels of calculation, the difference in the activation barrier height being insensitive to the level, 13.0 and 14.7 kcal/mol at the RHF/I//RHF/I and the MP2/I//RHF/I levels, respectively. At the more reliable MP2/I//RHF/I level, path 1 has no activation energy, consistent with the experimental result that the reaction is fast.[3] When the activation energy at the RHF level is small, it can become negative at the correlated

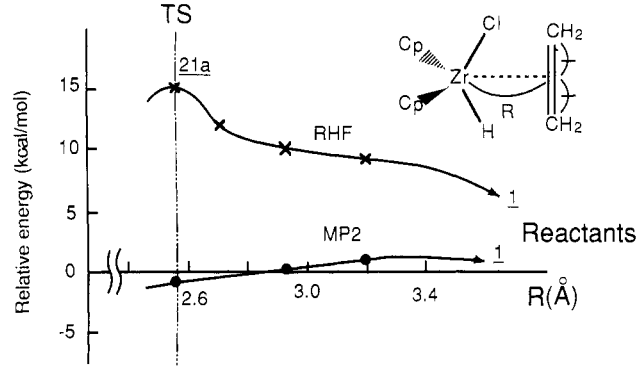

Figure 4. RHF/I and MP2/I potential energy profiles at RHF optimized geometries at fixed values of the $Zr-C_2H_4$ distance R, relative to the isolated reactants. TS represents the distance R in the true RHF/I transition state geometry.

level if calculated at the RHF transition state structure.[30] In such a case, the transition state has to be determined at the correlated level to obtain correct energetics. Instead, to obtain a better overall energy profile, we carried out the RHF/I geometry optimization at a few fixed values of the distance R between Zr and the C=C midpoint and calculated the MP2/I energy at each RHF/I optimized structure. The results in Figure 4 show that the MP2/I energy, relative to the reactants, is positive at R = 3.2 Å and therefore there must exist a transition state at a long distance with a very small activation energy. The barrier is so small that it may disappear when the zero-point vibration correction is taken into account. One can also see, as discussed before, that there is no ethylene complex in this region. Note that, as shown later, the MP2/I//RHF/I calculations for reaction 4 give the qualitatively same potential energy profile as the more reliable MP2/III//MP2/III calculations.

In transition metal ethyl complexes, especially for cationic complexes, one often finds agostic interactions a donative interaction from a β C—H bond to a metal, which makes the metal—C—C angle abnormally small and the metal—H distance short. For instance, Jordan et al. have found a β C—H agostic interaction in $(C_5H_4Me)_2Zr(CH_2CH_2R)(PMe_3)^+$ by X-ray diffraction.[31] In the present direct products, **31a** and **32a**, the Zr—C—C angles are larger than a tetrahedral angle and the Zr—H distance is over 3 Å. Therefore one may conclude that the agostic interaction does not exist here. In this neutral complex with the less electronegative Zr atom, the lowest unoccupied (LU) MO has a higher energy and therefore the donative interaction would be more difficult to take place than in cationic complexes, where the RHF optimization actually gave an agostic interaction.[12] Experimentally, in several neutral alkyl and vinyl Zr complexes, for instance, $Cp_2Zr(Cl)CH_2CH_2Ru(PMe_3)_2(Cp)$[32] and $Cp_2Zr(C(SiMe_3)=CHPh)X$,[33] the agostic interaction has been found to take place. In addition, theoretical calculations have shown that the electron correlation effect enhances the agostic interaction.[34] Therefore, we determined the structure of one of the products, **32a**, at the MP2/I level. The resultant structure shown in Figure 5 demonstrates clearly the

(30) Koga, N.; Morokuma, K. *J. Phys. Chem.* **1990**, *94*, 5454.
(31) Jordan, R. F.; Bradley, P. K.; Baenziger, N. C.; LaPointe, R. E. *J. Am. Chem. Soc.* **1990**, *112*, 1289.
(32) Bullock, R. M.; Lemke, F. R.; Szalda, D. J. *J. Am. Chem. Soc.* **1990**, *112*, 3244.
(33) Hyla-Kryspin, I.; Gleiter, R.; Krueger, C.; Zwettler, R.; Erker, G. *Organometallics* **1990**, *9*, 517.
(34) Weiss, H.; Haase, F.; Ahlrichs, R. *Chem. Phys. Lett.* **1992**, *194*, 492.

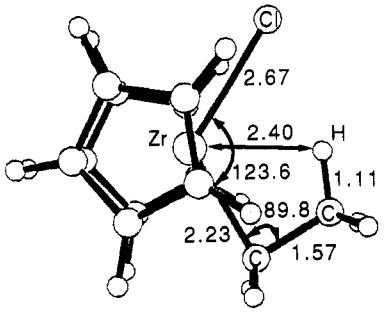

32a'

Figure 5. MP2/I optimized geometry of the direct product, **32a'**, for path 2 of the hydrozirconation of ethylene. Distances and angles are in Å and deg, respectively.

evidence of agostic interaction: the small Zr—C—C angle of 89.8°, the long C—H bond length of 1.11 Å, and the short Zr—H distance of 2.40 Å. The MP2/I energy calculations show that this agostic MP2/I structure is 8 kcal/mol more stable than the nonagostic RHF/I structure, whereas the latter is 11 kcal/mol more stable at the RHF level, with the correlation effect stabilizing the agostic structure by 19 kcal/mol. Due to the agostic interaction the eclipsed ethyl complex such as **32a** is often more stable than the staggered ethyl complex such as **42a** in which the agostic interaction is structurally difficult to take place.[23b] Therefore, the direct product, **32a'**, would also be the thermodynamic product for path 2. We did not investigate further the agostic interaction, but we expect that the agostic interaction stabilizes the direct products for paths 1 and 2 by a similar extent and thus the β-agostic direct product **31a'** is the thermodynamic product for path 1 as well.

Before going into detailed discussion of the interaction between the reactants during the reaction, we show in Figure 6 the orbital correlation diagram for the transition state **21a** for path 1. The geometries of the fragments, $Cp_2Zr(H)Cl$ and C_2H_4, are those at **21a**, and the orbitals and their energies are the actual RHF results. The LUMO 30a' of $Cp_2Zr(H)Cl$ extends toward the bisector of the ClZrH angle. Since the highest occupied (HO) MO and high-lying occupied orbitals are rather complicated, the interaction pattern is not very simple and requires some detailed analysis to be presented below.

In order to investigate the reason why the barrier for path 1 is lower than that for path 2, we have carried out the energy decomposition analysis (EDA)[35] for the RHF activation energy, as shown in Table I. As shown above, the electron correlation effect does not change the energy difference between the two paths. In this analysis, the activation energy is divided into two parts: the deformation energy, the energy required to deform each reactant from its equilibrium geometry to that of the transition state, and the interaction energy between the two deformed reactants at the transition state. The latter is further decomposed into the electrostatic interactions (ES), the exchange repulsion (EX), the donative interaction (CT-PLX) from olefin to the $Cp_2Zr(H)Cl$, the back-donative interaction from the Zr complex to olefin, and the residual term (MIX).

Table I shows that the difference between path 1, **21a**, and path 2, **22a**, in the RHF activation energy, 13.0 kcal/mol, is mainly determined by the difference in the

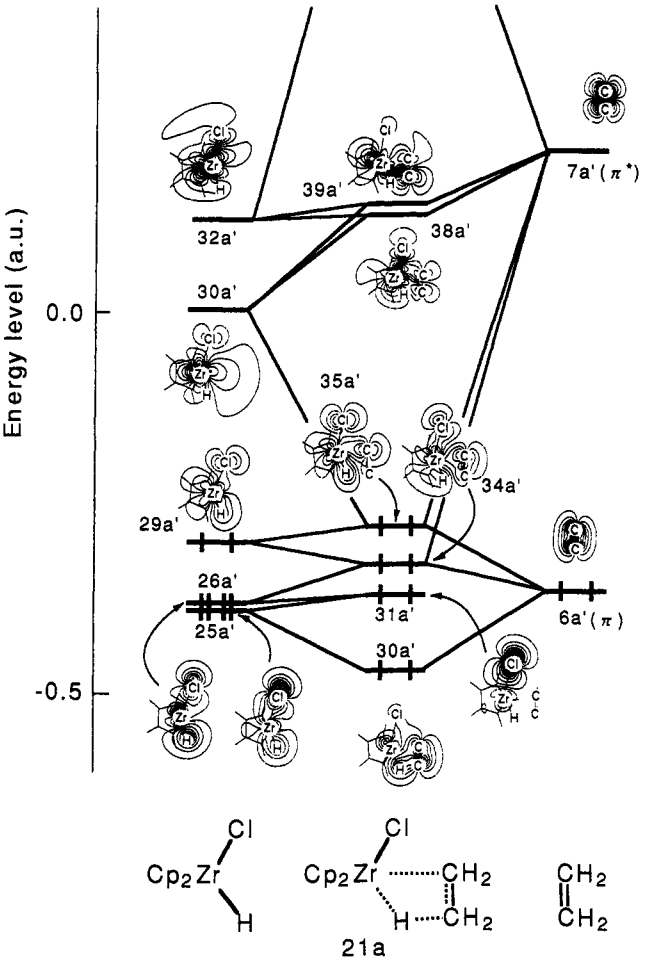

Figure 6. Orbital interaction diagram at the transition state **21a**.

deformation energy (8.0 kcal/mol), supplemented by that in the interaction energy (5.0 kcal/mol). The deformation energy contribution comes essentially from that of the Zr complex (9.0 kcal/mol); the distortion of the Zr complex costs substantially less for path 1 than for path 2. One of the reasons for the smaller deformation energy for path 1 is presumably the smaller repulsion between the hydride and the chloride ligand, the HZrCl angle being 71.1°. Another possible reason may be that the Zr–H bond at the transition state for path 1, **21a**, is stronger. In Figure 7 are shown the LUMO and the next LUMO for Cp_2ZrCl^+, with which the hydride is considered to make a bond through electron donation. These orbitals were calculated for the Cp_2ZrCl^+ fragment at **21a**. Those for the path 2 transition state (**22a**) are very similar. The LUMO, more favorable energetically for interaction with the orbital energy of –0.140 au, extends more toward the direction of the hydride of **21a** than **22a**. The next LUMO, less favorable energetically for interaction with its energy of –0.118 au, is more suitable for Zr–H bonding in **22a** than in **21a**. Therefore, the Zr–H interaction would be stronger and thus the energy of the deformed fragment would be lower for **21a** than for **22a**. The figure similar to Figure 7, calculated with the extended Hückel method has been reported in analyzing the interaction between Cp_2ZrCl^+ and $CH_2PH_2^-$ and between Cp_2TiCl^+ and CH_3CO^-.[36]

The interaction energy also makes path 1 more favorable. Table I shows that every interaction component has an

(35) Kitaura, K.; Morokuma, K. *Int. J. Quantum Chem.* **1976**, *10*, 325.

(36) (a) Hofmann, P.; Stauffert, P.; Schore, N. E. *Chem. Ber.* **1982**, *115*, 2153. (b) Tatsumi, K.; Nakamura, A.; Hofmann, P.; Stauffert, P.; Hoffmann, R. *J. Am. Chem. Soc.* **1985**, *107*, 4440.

Table I. Decomposition of the Activation Energies at the RHF Level (kcal/mol)

	$Cp_2Zr(H)Cl\ C_2H_4$			$Cp_2Zr(H)Cl + C_2H_2$		$Cp_2Zr(CH_3)Cl + C_2H_4$
	path 1		path 2	path 1	path 2	path 1
	21a	**21a'**[b]	**22a**	**21b**	**22b**	**21c**
activation energy	+15.1	+15.3	+28.1	+16.0	+29.0	+44.8
deformation energy						
total	+22.5	+22.5	+30.5	+23.9	+31.6	+60.7
Zr complex	+16.1	+16.1	+25.1	+14.4	+23.8	+43.1
olefin	+6.4	+6.4	+5.4	+9.5	+7.8	+17.6
interaction energy						
total	−7.4	−7.2	−2.4	−7.9	−2.6	−15.9
ES	−70.8	−58.5	−57.5	−65.6	−54.7	−90.7
EX	+130.0	+106.5	+106.7	+118.4	+99.2	+173.8
CTPLX						
Zr←olefin	−32.1	−27.3	−23.6	−32.1	−21.3	−44.6
Zr→olefin	−34.5[a]	−28.1[a]	−28.5	−29.3	−25.8	−54.4
MIX			+0.5	+0.7	0.0	0.0

[a] Sum of the last two terms. Their separation failed due to the SCF inconvergence. [b] The distance between Zr and the C=C midpoint is 2.635 Å. Other geometrical parameters are fixed to those of **21a**.

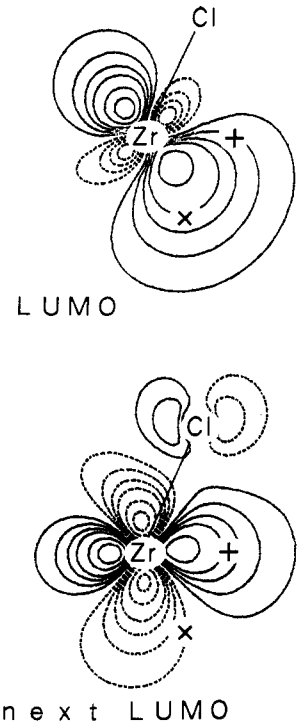

Figure 7. Contour maps of the LUMO and next LUMO of Cp_2ZrCl^+ at the path 1 transition state geometry. The position of the hydride is in the path 1 transition state shown by x, and that in path 2 is shown by +. Contour heights are ±0.025, ±0.05, ±0.1, ±0.15, ±0.20, and ±0.25 au.

absolute value larger for path 1 than for path 2; this is because the transition state for path 1 (**21a**) is later, tighter, and thus more strongly interacting than that for path 2 (**22a**). In this situation, it is not easy to extract the most important component. In such a case, an acceptable protocol is to analyze the interaction energy calculated at the adjusted structures with the comparable "interfragment distance", i.e. where the exchange repulsion EX is comparable.[37] We carried out the EDA analysis for path 1 at several distances R between Zr and the C=C midpoint with the other geometrical parameters fixed to those of **21a**. We found that at R = 2.635 Å the EX term is comparable to that of **22a** as shown for **21a'** in Table I.

The ES and CTPLX(Zr → C_2H_4) terms for **21a'** are also similar to those for **22a**, whereas CTPLX(Zr ← C_2H_4) for **21a'** is more negative than that for **22a** by 3.7 kcal/mol. For **21a'**, the newly-forming Zr—C and C—H distances are 2.62 and 1.78 Å, respectively, which are shorter by 0.09 and 0.06 Å, respectively, than those in **22a**. Reflecting this shorter Zr—C distance, CTPLX(Zr ← C_2H_4) is more negative. In other words, though the distance between the Zr fragment and ethylene in **22a** is longer, EX, an indicator of the interfragment contact, is similar to that for **21a'**. This suggests that the site of the Zr fragment attacked in path 2 is more congested; it is easier for ethylene to approach the Zr atom through path 1 than through path 2.

In addition, in order to understand the nature of interactions at the transition states in more detail, we carried out the density decomposition, in which the difference density between the transition state and the deformed, isolated reactants was decomposed into terms corresponding to those in EDA. As shown in Figure 8, the results for both paths are qualitatively similar. Therefore, here we discuss only the difference density for path 1.

In the total difference map, the electron density increases between Zr and the ethylene α carbon, showing that the new Zr–C bond has partially formed. The donation term CTPLX(Zr←C_2H_4) accumulates electrons at the region between ethylene α carbon and the Zr atom, where the LUMO of $Cp_2Zr(H)Cl$ (30a' in Figure 6) extends as shown. Electron donation from the ethylene π orbital to this LUMO in CTPLX(Zr←C_2H_4) is the principal origin of the new Zr–C bond formation.

On the other hand, the electron density between the hydride of the Zr fragment and the ethylene β carbon decreases drastically, as shown in the Δq_{total}. This is different from the case of usual bond formation in which the electron density increases at the newly forming bond region as in the Zr–C bond formation discussed above. CTPLX(Zr→C_2H_4) + MIX actually accumulates the electron density between the hydride and the β carbon mainly through electron donation from the HOMO of the Zr fragment, having a large lobe around the Zr–H bond, to the ethylene π^* orbital. However, EX decreases the electron density between the β carbon and the hydride, and CTPLX(Zr←C_2H_4) transfers electrons from the partially formed β C–H bond to the other parts of the Zr fragment. Without these synchronized changes of electronic distribution from the isolated, deformed reactants,

(37) (a) Sakaki, S.; Kitaura, K.; Morokuma, K. *Inorg. Chem.* **1982**, *21*, 760. (b) Sakaki, S.; Kitaura, K.; Morokuma, K.; Ohkubo, K. *Inorg. Chem.* **1983**, *22*, 104. (c) Nakamura, E.; Miyachi, Y.; Koga, N.; Morokuma, K. *J. Am. Chem. Soc.* **1992**, *114*, 6686.

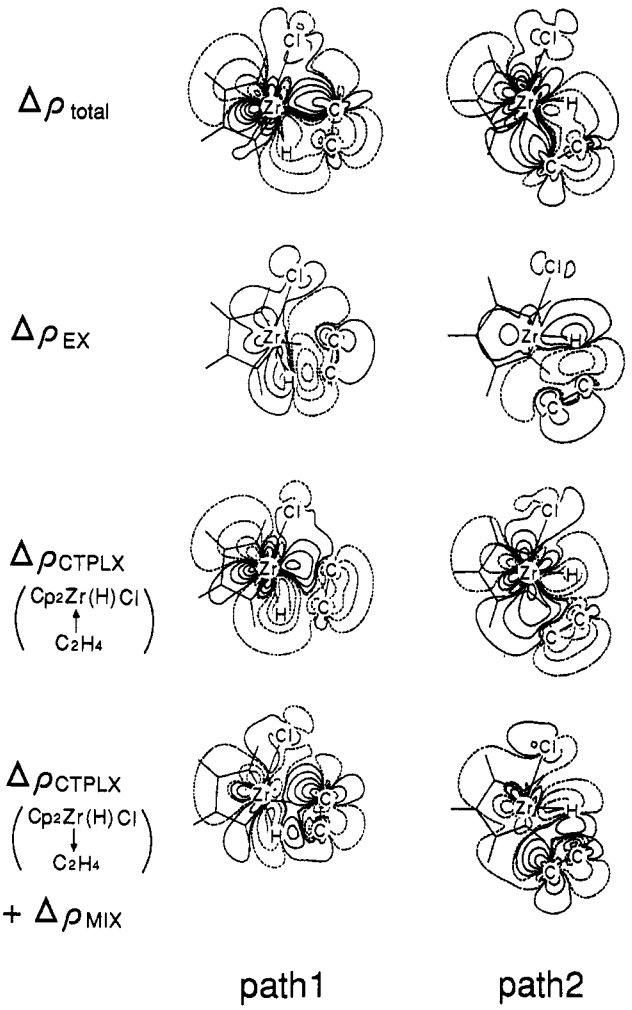

Figure 8. Contour maps of the total end EDA component difference density between transition states, **21a** and **22a**, and the reactants. Solid and broken lines indicate an increase and decrease, respectively, at the transition state.

too many electrons, more than 2, would distribute at the partially formed β C–H bond, resulting in serious exchange repulsion. Although the electron density between the hydride and the β carbon decreases, the bonding interaction between them is enhanced.

In summary of this section, path 1 is more favorable than path 2 kinetically as well as thermodynamically. This is predominant because deformation leading to the transition state structure is easier for path 1 than for path 2 and partly because path 1 is less crowded. These points could be clearer, when the potential energy profiles for reaction 1 are compared with those for reaction 4 in the next section. Note that the preference of path 1 over path 2 is different from the preference of CO attack in CO insertion, $CO+Cp_2Zr(CH_3)_2$, studied by the extended Hückel calculations.[36] Presumably, the end-on attack of CO does not suffer from the steric hindrance, different from the side-on attack of ethylene in path 2 of the present reaction.

5. Model Hydrozirconation of Ethylene by Cl_3ZrH

For reaction 4, the model hydrozirconation of ethylene by the chloride analogue of the zirconocene complex, Cl_3ZrH, the structures of Cl_3ZrH determined at the several levels are shown in Figure 9 and those for the ethylene complex (**11d** and **12d**), the transition state (**21d** and **22d**), and the direct product (**31d** and **32d**) are in Figure 10. The

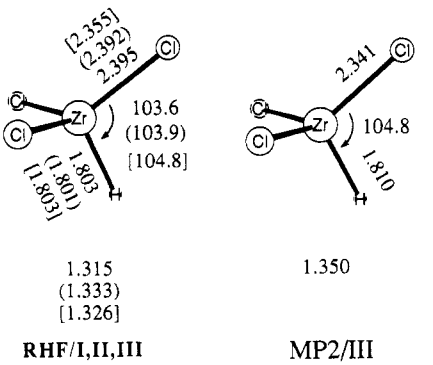

Figure 9. Geometries of Cl_3ZrH optimized at (a, left) the RHF and (b, right) the MP2/III levels. The geometrical parameters for the RHF geometry are with the basis set I. Those in parentheses and square brackets are with the basis sets II and III, respectively. Distances and angles are in Å and degrees, respectively.

energetics obtained are summarized in Table II. We have not studied the final product.

As shown in Figure 9, the HZrC angle changes within only 1°, when the computational method changes from the RHF/I to the MP2/III level. On the other hand, the polarization function shortens the Zr–Cl bond by 0.04 Å and the electron correlation effect furthermore by 0.01 Å. Though the RHF/I Zr-Cl distance of 2.55 Å in Cp_2ZrCl_2 is 0.1 Å longer than the experimental bond distance, the electron correlation and the polarization function on Cl would give better agreement.

As to the potential energy profiles for path 1 and 2, we first discuss that for path 1 calculated at the RHF level. At the RHF/I and the RHF/II levels, the ethylene complex, **11d**, was located on path 1. Note that at the RHF/II level this complex is less stable than the isolated reactants and thus there must exist a transition state between **11d** and the reactants. However, when the polarization functions are augmented, **11d** disappeared at the RHF/III level, suggesting that at the RHF level the ethylene complex exists as a result of basis set superposition error (BSSE).

At the RHF level with all the basis sets, we found that the four-centered transition state for path 1, **21d**, exists. Though its relative energy depends on the basis set used, the structure is not very sensitive to the basis sets. The largest difference of 0.1 Å is seen in the C^{β}–H bond distance, whereas the other differences are much smaller. Because of the BSSE, **21d** has a low relative energy at the RHF/I level, the activation energy relative to the ethylene complex being only 0.4 kcal/mol. With the better basis sets, II and III, the relative energy of **21d** increases, resulting in an absence of the ethylene complex at the RHF/III level.

The electron correlation effect changes the potential energy profile drastically. At the MP2/III level, the transition state, **21d**, as well as the ethylene complex, **11d**, dissapears. The MP2/III geometry optimization of the ethylene complex starting with the RHF/II structure converged to the structure of the product. Thus, the reaction is downhill, similar to the MP2/I//RHF/I calculations for path 1 of reaction 1. The electron correlation also changes the structure of the product, **31d**. At the MP2/III level, **31d** has an agostic ethyl group with the small ZrCC angle of 96.5°, the long β C–H bond of 1.110 Å, and the short Zr–H distance of 2.54 Å, while at the RHF level such an agostic interaction does not take place. The electron-withdrawing Cl trans to the agostic C–H bond in **31d** enhances the C–H→Zr donative interaction, the origin

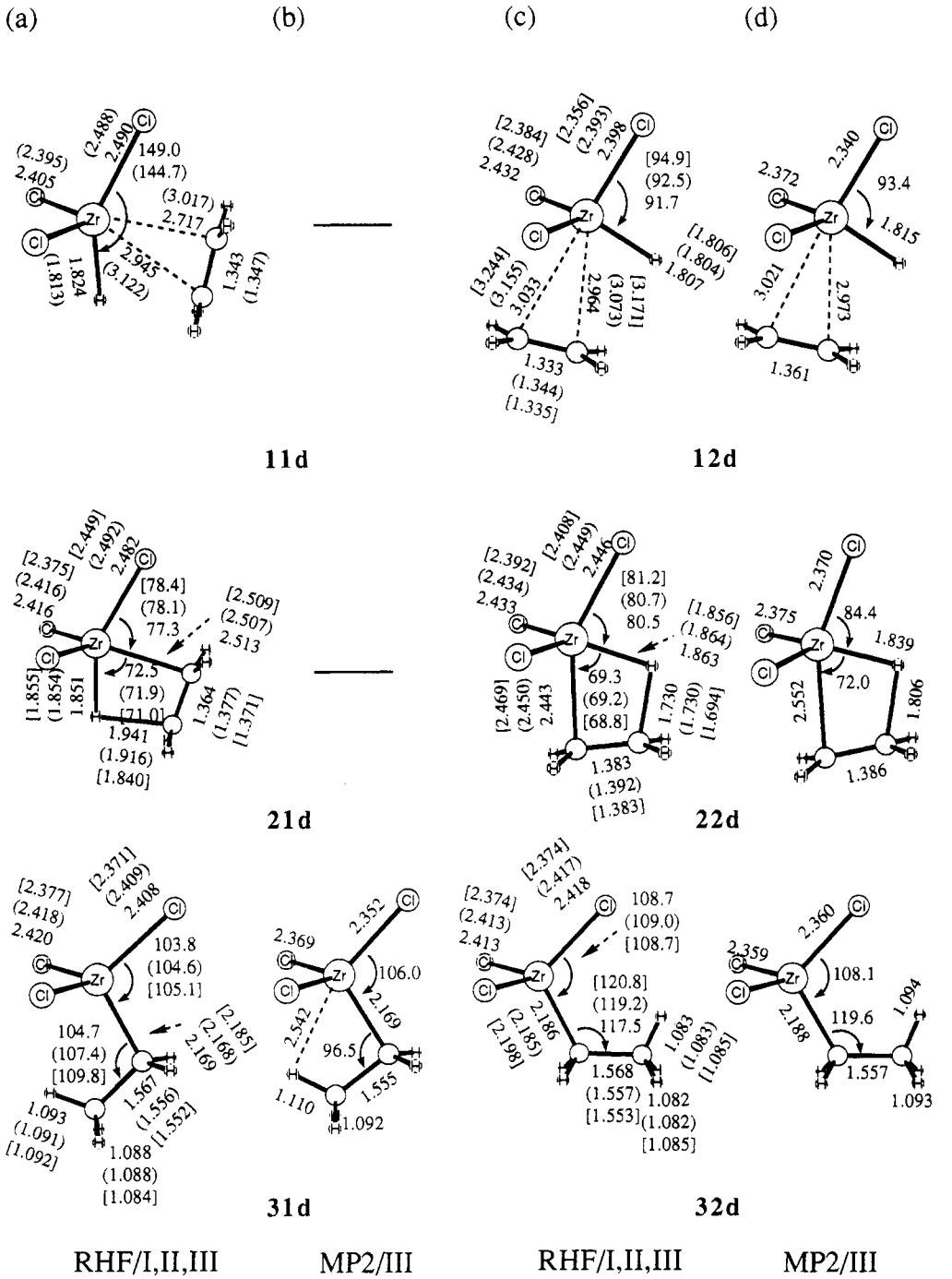

Figure 10. Geometries, optimized at the RHF and the MP2/III level, of ethylene complexes (**11d** and **12d**), transition states (**21d** and **22d**), and products (**31d** and **32d**) for paths 1 and 2, respectively, of the model hydrozirconation of ethylene with Cl_3ZrH. Distances and angles are in Å and deg, respectively. The geometrical parameters for the RHF geometry are with the basis set I. Those in parentheses and square brackets are with the basis sets II and III, respectively.

of the agostic interaction, though it is weak, and thus the correlation effect is required to realize this interaction.

Next, the potential energy profile for path 2 is discussed. For path 2 we determined at all the levels the structures of the ethylene complex, **12d**, and the transition state, **22d**. The ethylene coordination in **12d** is weak, judged from the C=C distance stretched by only 0.01–0.02 Å upon coordination. Similar to path 1, the structure of **22d** is not sensitive to the basis set used at the RHF level. The correlation effect also does not change the structure of **22d** very much. These are true of the structure of the product, **32d**, as well; even at the MP2/III level an agostic interaction does not take place.

While the total energies of these stationary points are dependent on the computational methods, the energy of **22d** relative to **12d** at the RHF level is 8-9 kcal/mol and not sensitive to the basis sets. The electron correlation decreases the activation barrier relative to **12d** to be 3.5 kcal/mol at the MP2/III level.

This potential energy profile for path 2 is different from that path 1 which is downhill in the point that there is the ethylene complex on path 2. If the RHF transition states for paths 1 and 2 are compared in energy, the transition state for path 1, **21d**, which exists only at the RHF levels, is found to be less stable than that for path 2, **22d**, different from reaction 1. However, path 1 is downhill, because of the absence of an ethylene complex, and path 2 requires the moderate activation energy relative to the ethylene complex, **12d**. Therefore, one can conclude that path 1 is more favorable than path 2. There are two possible reasons

Table II. Energies (kcal/mol) at the Various Levels for the Reaction $Cl_3ZrH + C_2H_4 \rightarrow Cl_3ZrC_2H_5$ Relative to the Reactants[a]

mehod	ethyelene complex	transition state	product
	Path 1		
RHF/I//RHF/I	−3.4	−3.0	−40.6
RHF/II//RHF/II	2.7	4.1	−34.8
RHF/III//RHF/III		8.8	−29.9
MP2/III//MP2/III			−45.3
MP2/I//RHF/I	−8.7	−9.5	−45.0
MP2/III//RHF/I	−4.1	−5.1	−45.8
	Path 2		
RHF/I//RHF/I	−12.3	−4.5	−32.8
RHF/II//RHF/II	−6.1	3.1	−32.3
RHF/III//RHF/III	−3.7	7.7	−27.7
MP2/III//MP2/III	−11.5	−7.9	−41.9
MP2/I//RHF/I	−16.2	−11.4	−41.6
MP2/III//RHF/I	−11.3	−8.1	−42.8

[a] The total energies of the reactants are −1496.366 21, −1502.920 90, −1503.019 89, −1503.870 36, −1496.839 74, and −1503.865 79 hartrees, at the RHF/I//RHF/I, RHF/II//RHF/II, RHF/III//RHF/III, MP2/III//MP2/III, MP2/I//RHF/I, and MP2/III//RHF/I levels, respectively.

why **12d** is so stable, compared with the ethylene complex for path 1, **11d**. One reason is that the change of the HZrCl angle in **12d** from Cl_3ZrH is smaller than that in **11d** and thus the deformation energy required for complexation is smaller. In **12d** the change of that angle is −12° (RHF/I), whereas it is +45° (RHF/I) in **11d**. The more detailed analysis will be shown later. Also, the trans effect of electron-withdrawing Cl would assist the ethylene complexation by enhancing electron donation from ethylene to the Zr atom, similar to what is seen in the agostic interaction.

In reaction 1, we found that path 1 is much more favorable than path 2; the transition state for path 2, **22a**, is 13–15 kcal/mol less stable than that for path 1, **21a**. Compared with **22a**, **22d** is relatively stable and has an energy comparable to **21d**. This and the existence of the ethylene complex, **12d**, show that the replacement of Cp by Cl makes it easier for ethylene to approach the Zr complex through path 2. This is also seen in the Zr–C^{α} bond distance in the transition states; while that in **22a** is 2.71 Å, that in **22d** is 2.44 Å (RHF/I). Similar to the ethylene complex, the small change of the HZrCl angle at **22d** from Cl_3ZrH could make a contribution to the relative stability of **22d**. Thus, we calculated at the RHF/I level and compared the deformation energy for the Cl_3ZrH fragment in **21d** and **22d**. That for **21d** is 17.6 kcal/mol, 1.5 kcal/mol larger than that for **21a**, whereas that for **22d** is 11.0 kcal/mol, 14.1 kcal/mol smaller than that for **22a**. The HZrCl angle in **21d** is about 150°, which is about 10° larger than that in **21a**. Presumably, with the smaller Cl this angle opens to decrease the steric repulsion between the Zr complex and ethylene. With the smaller Cl and thus being less crowded, the C^{α}ZrCl angle in **22d** could open more than that in **22a**. Consequently, to decrease the deformation energy of Cl_3ZrH, this angle opens to be about 150°, 10° larger than that in **22a**. Therefore, one can say that path 2 of reaction 4 is less crowded and more attractive, compared with that of reaction 1, because of the smaller size of Cl than of Cp. One can also say that in reaction 1 the larger size of the Cp ligands makes path 1 definitely more favorable than path 2.

Furthermore, we carried out the energy calculations at the MP2/I and the MP2/III levels for the RHF/I optimized structures, in order to check the computational method

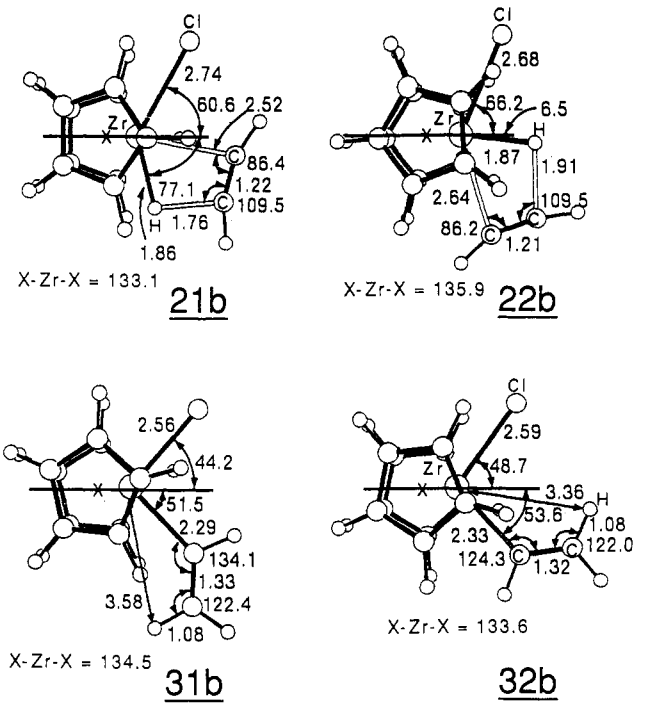

Figure 11. RHF/I optimized geometries at the transition states (**21b** and **22b**) and products (**31b** and **32b**) for the hydrozirconation of acetylene. Distances and angles are in Å and deg, respectively.

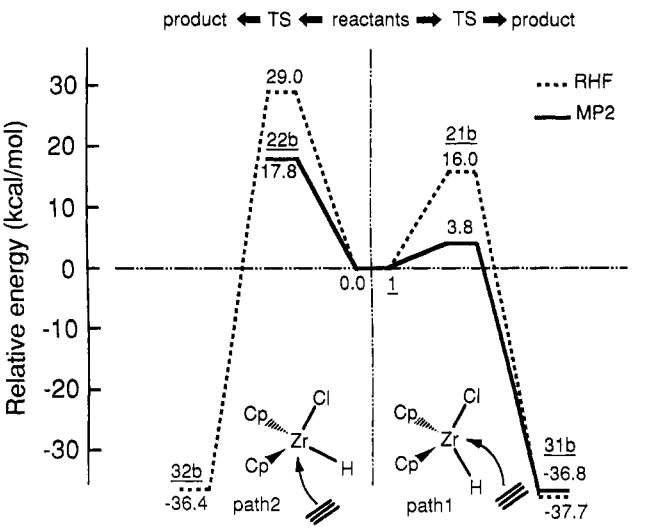

Figure 12. Relative potential energy profiles from the reactants for the hydrozirconation of acetylene.

for reaction 1. The results shown in Table II demonstrate that the MP2/I as well as the MP2/III calculations at the RHF/I optimized structures gave results quite similar to those of the MP2/III//MP2/III calculations. For instance, the transition state for path 1, **21d**, is more stable than the ethylene complex, **11d**, and thus path 1 is downhill. These results show that the methods used for reaction 1 are acceptable.

6. Hydrozirconation of Acetylene

As in reaction 1 for ethylene, there are also two paths for the reaction of acetylene, reaction 2. The RHF/I optimized geometries and RHF/I//RHF/I and MP2/I//RHF/I relative energies of these paths are shown in Figures 11 and 12, respectively.

The comparison of bond distances between the transition states for reactions 1 and 2, between **21b** and **21a**

for path 1 and between **22b** and **22a** for path 2, is interesting. The newly formed Zr–C distances at **21b** and **22b** for acetylene reactions are shorter than those at **21a** and **22a** for ethylene reactions by 0.02–0.07 Å, the newly formed C–H distances are longer by 0.05–0.07 Å, and the breaking Zr–H bond distances are nearly the same. One can say that the transition state for reaction 2 is nearly at the same stage of reaction as that for reaction 1. The former transition state is more asynchronous in the points that the Zr–C bond formation is more advanced and that the C–H bond formation is less so than in the latter. This asynchronism is probably related to the slightly smaller repulsion on the Cp hydrogen atom caused by the acetylene hydrogens than that caused by the ethylene hydrogens. The latter hydrogens are out of the symmetry plane.

For the optimized geometries of the products, **31b** and **32b**, there is no agostic interaction. As discussed in sections 4 and 5, electron correlation would cause the agostic interaction. Although the X–Zr–X angles of **31a** and **31b** are almost the same, 134.2 and 134.5°, respectively, the X–Zr–C angle of **31b**, 104.0°, is smaller by 1.4° than that of **31a**, 105.4°; this reflects the smaller contact of the Cp ligands with the vinyl hydrogen atoms in **31b** than that with the ethyl hydrogen in **31a**.

The MP2, as well as RHF, activation energy for path 1 is smaller than that for path 2 by about 14 kcal/mol, as in reaction 1 for ethylene. The MP2 barrier for path 1 of reaction 2 is small but positive, different from reaction 1 in Figure 3. The difference of 0.9 kcal/mol in the RHF barrier between reactions 1 and 2 is quite small and the correlation energy increases the difference slightly. This small difference is, as shown in Table I, the consequence of small contributions of differences in the deformation energy, ES, and CTPLX(Zr→C_2H_n).

The present results suggest that hydrozirconation of alkyne is intrinsically more difficult. Our results seem not to be in agreement with the experimental results,[3d] showing that alkyne is hydrozirconated much faster than alkene. However, the present theoretical results should not be compared directly with the experiments where substituted alkene and alkyne were used. The activation energy for the reaction of substituted alkenes would be higher than that for the reaction of substituted alkynes, because of the larger steric repulsion between the Cp ligands and the substituents.

Hydrozirconation of acetylene, reaction 2, is calculated to be more exothermic than that of ethylene, reaction 1. This is probably related to the fact that hydrogenation of acetylene giving ethylene is more exothermic than that of ethylene leading to ethane. The experimental standard heat of acetylene hydrogenation at 298.15 K is −42 kcal/mol and that of ethylene is −33 kcal/mol,[38] and the calculated energy (without vibrational correction) of the former hydrogenation is −52 (RHF/3-21G), −55 (RHF/6-31G*), −47 (MP2/6-31G*), and −48 (MP4/6-31G*) kcal/mol and that of the latter is −44 (RHF/3-21G), −44 (RHF/6-31G*), −41 (MP2/6-31G*), and −40 (MP4/6-31G*) kcal/mol. The calculated MP2 difference of 37.7–29.8 = 8 kcal/mol in energy of the hydrozirconation through path 1 is in good agreement with these differences. More favorable is the conversion of a CC triple bond and a σ bond (a H–H bond or a Zr–H bond) into a CC double bond and two σ bonds (two C–H bonds or a Zr–C and a C–H bond) than that of a double bond and a σ bond into a CC single bond and two σ bonds.

(38) *CRC Handbook of Chemistry and Physics*; Weast, R. C., Ed.; CRC Press, Inc.; Boca Raton, FL, 1987.

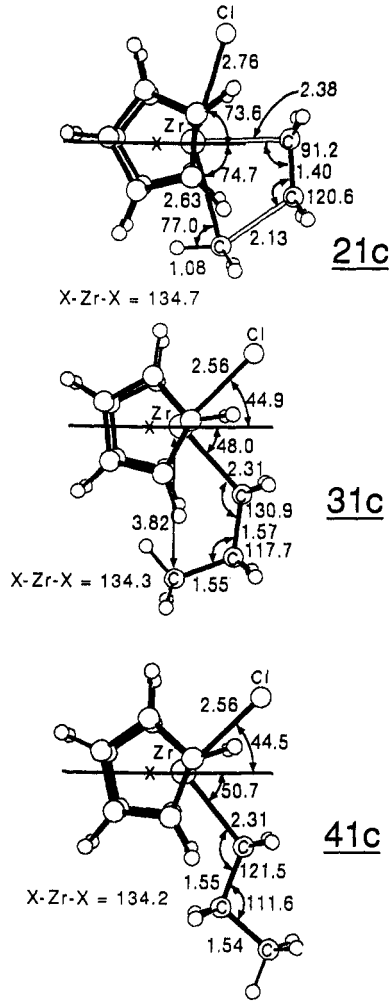

Figure 13. RHF/I optimized geometries at the transtion state **21c** and direct product **31c** for the insertion reaction of ethylene to the Zr–C bond. **41c** is the assumed geometry of the final product. Distances and angles are in Å and deg, respectively.

7. Insertion Reaction of Ethylene to the Zr–C Bond

In order to investigate the reason why insertion of the second olefin does not occur in hydrozirconation, we have studied the reaction of $Cp_2Zr(CH_3)Cl$ with ethylene, reaction 3, where CH_3 on Zr is a model for a longer alkyl group. Here we have restricted geometry optimization only to path 1, which is expected to be more favorable than path 2, as in the hydrozirconation discussed above.

The RHF/I optimized structures of transition state **21c** and direct product **31c** are shown in Figure 13. The newly forming Zr—C distance in **21c** is substantially (0.16 Å) shorter and the breaking C=C distance is 0.03 Å longer, compared with those in **21a**, indicating that the transition state for this reaction, **21c**, is later and tighter than that for reaction 1, **21a**. Direct product **31c** shows no sign of an agostic interaction, although again the electron correlation may make a weak γ-agostic interaction take place.

The energetics shown in Figure 14 indicates that, unlike reaction 1 to the hydride complex where the MP2/I//RHF/I barrier was nearly zero, reaction 3 to the alkyl complex requires a high activation barrier of about 27 kcal/mol at the MP2/I//RHF/I level. This high activation barrier to

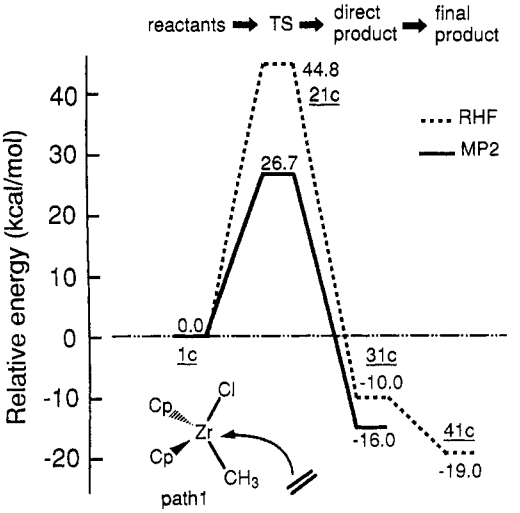

Figure 14. Relative potential energy profiles from the reactants for the insertion reaction of ethylene into the Zr–C bond.

insertion into a Zr–C bond is consistent with the lack of succeeding insertion in the hydrozirconation experiment. A comparison of the interaction energy terms between **21a** and **21c** in Table I shows clearly that this higher activation energy is ascribed to the large deformation energy of the zirconium fragment. This deformation is due to the change of orientation of the methyl ligand; at the transition state the CH_3 group has to rotate its pseudo C_{3v} axis substantially to gain a favorable interaction energy with an olefin carbon, which in turn destablizes the energy of the $Cp_2Zr(CH_3)Cl$ fragment by the loss of the CH_3–Zr bond. A three-center interaction of a directional carbon sp^3 hybrid orbital with the Zr atom and an ethylene carbon atom is less favorable than that of a spherical hydrogen atom. One notes also in Table I that **21c**, the later and tighter transition state, has all the interaction energy terms larger in magnitude than **21a**.

The energy of the final product, **41c**, was calculated at the assumed geometry in which the trans ethyl hydrogen atom in **41a** was replaced by CH_3 with geometry taken from the optimized propane geometry. The lower bound of relaxation energy of the product propyl complex, the energy difference between **31c** and **41c** of about 9 kcal/mol, is substantial. After the relaxation, the exothermicity for reaction 3 is about 5 kcal/mol smaller than that for reaction 1.

The activation barrier to ethylene insertion into the M–CH_3 bond of cationic complex $X_2MCH_3^+$, a model reaction of olefin polymerization, has been calculated to be much lower than those for hydrozirconation by the present model compound.[11,12] For instance, the activation barrier relative to the ethylene complex for ethylene insertion to $(H_2SiCp_2)Zr(CH_3)^+$ and $Cl_2Ti(CH_3)^+$ was calculated at the MP2 level to be 6 and 4 kcal/mol, respectively.[12] The energy decomposition analysis at the transition state for reaction of C_2H_4 with $Cl_2TiCH_3^+$ [12a] shows that the deformation energy of 18 kcal/mol for the Ti fragment is much smaller than that, 61 kcal/mol, for the $Cp_2Zr(CH_3)Cl$ fragment in reaction 3. In cationic complexes, the strong agostic interaction takes place at the transition states; one of the C–H bonds interacts with the electron deficient central metal through electron donation from the C–H bond and is stretched to be 1.12 Å.[12] This attractive interaction reduces the deformation energy. In neutral transition state **21c**, however, the agostic interaction does not take place; the distance of the C–H bond which might interact with the Zr atom is 1.084 Å and normal. In addition, in **21c** the CH_3–Zr–Cl angle has to be opened more than that in **21a** and **21b** because of the steric hindrance. Thus, overall, in cationic reactants bending of the Zr–CH_3 bond is very soft and thus the deformation is easier and the barrier is smaller than in neutral reactants.

8. Conclusion

Our conclusion may be summarized as follows. In hydrozirconation, path 1 is the favorable reaction path. This is mainly determined by the difference in deformation energy of the Zr complex between two paths; the distortion of the Zr complex for path 1 is easier than that for path 2, because of a smaller repulsion between the hydride and the chloride ligand and also of a stronger Zr–H bond. The calculated activation barrier for path 1 for hydrozirconation of ethylene is very small, consistent with the experimental result that the reaction is fast. The product has an agostic interaction, which is only realized when the geometry is optimized at the correlated MP2 level. Preference of path 1 is unchanged upon replacement of Cp by Cl, path 1 being downhill. In reactions of Cl_3ZrH with C_2H_4, however, the smaller size of the Cl ligands makes the approach through path 2 not very unfavorable and the ethylene complex is a stable intermediate, from which the moderate activation energy is obtained.

Hydrozirconation of acetylene is intrinsically more difficult than that of ethylene. However, substituted alkenes will have a higher activation energy than alkynes, because of larger steric repulsion between the Cp ligands and the substituents. The second insertion of ethylene in hydrozirconation, i.e. the insertion of ethylene into the Zr–C bond of $Cp_2Zr(R)Cl$, is difficult, because the directional sp^3 hybrid orbital of a carbon atom is more difficult to interact simultaneously with Zr and olefin at the transition state.

Acknowledgment. Part of the numerical calculations were carried out at the Computer Center of IMS. J.E. was a Visiting Research Fellow at IMS when this work was carried out. This study was supported in part by grants-in-aid from the Ministry of Education, Culture, and Science of Japan.

OM920645A